Proceedings of the 15th International Symposium on the
Packaging and Transportation of Radioactive Materials
PATRAM 2007
October 21-26, 2007, Miami, Florida, USA

ON THE DUCTILITY VARIATION OF DUCTILE CAST IRON FOR SPENT NUCLEAR FUEL PACKAGES AND ITS CORRELATION WITH CASTING DEFECTS AND MATERIAL MICROSTRUCTURE

Vratko Vokál **Karl-Fredrik Nilsson** **Philip Minnebo**
European Commission, DG-JRC, Inst. For Energy, P.O Box 2, 1755 ZG, Petten, The Netherlands

ABSTRACT

The paper describes a study to correlate the variation in ductility in ductile cast iron to casting defects and microstructure. A large set of tensile and fracture specimens taken from three inserts for the Swedish KBS-3 programme were tested. About half the tensile specimens were analysed by microstructural analysis methods to identify and size defects and microstructural variations. The elongation at fracture was reduced by casting defects in the form of magnesium-oxide films and to a lesser extent by the graphite properties. An elastic-plastic probabilistic fracture mechanics model that relates the variation in ductility to the size and shape of casting defects is presented. The agreement between computed and measured results is quite good.

INTRODUCTION

Ductile cast iron is used for containers for spent nuclear fuel and radioactive waste. Its attractive properties include high ductility and strength, a relatively low price and that large components can be cast. Ductile cast iron is, however, a very complex material and material properties may vary significantly due to inherent variations in microstructure and casting defects. Containers for radioactive waste and spent nuclear fuel need to fulfill strict quality requirements to eliminate the risk of failure during operation. This requires definition of defect acceptance criteria and that their probability of detection is sufficiently high. This paper presents work performed in a study to relate the variation in ductility of the inserts for the Swedish copper/ductile cast iron canisters to defects and microstructure and how it affects the failure probability of complete canisters [1],[2],[3],[4]. The study was based on three inserts referred to as I24, I25 and I26 that had been manufactured by three different forgeries during the pilot stage of the Swedish programme. This paper deals specifically with the ductility variation. The outline of the paper is as follows. The statistical test plan and the results of the mechanical tests are first presented. This is followed by a description of the microstructural analysis of tested specimen to relate defects and microstructure to ductility. A probabilistic fracture mechanics model is then presented to correlate the size and shape of casting defects to variation in ductility.

EXPERIMENTAL WORK

Statistical Test Plan

Tensile, compression and fracture tests were performed on a large set of specimens, in accordance with standard test procedure [5],[6]. For each insert a slab from the solid bottom and

a slab from the top with fuel channels were cut out as shown in Figure 1 and used for specimen preparation. Specimens were taken at different locations and with different orientations of top and bottom. In total there were about 150 tensile, 50 fracture and 20 compression specimens with essentially the same cutting scheme for each inserts. Most tensile specimens had a diameter of 14 mm but some had 9 mm or 20 mm. The Joint Research Centre (JRC) and the Swedish Casting Association (SWECAST) performed tensile tests, JRC performed compression tests and JRC and Royal Institute of Technology (KTH) conducted three-point bend specimen fracture tests.
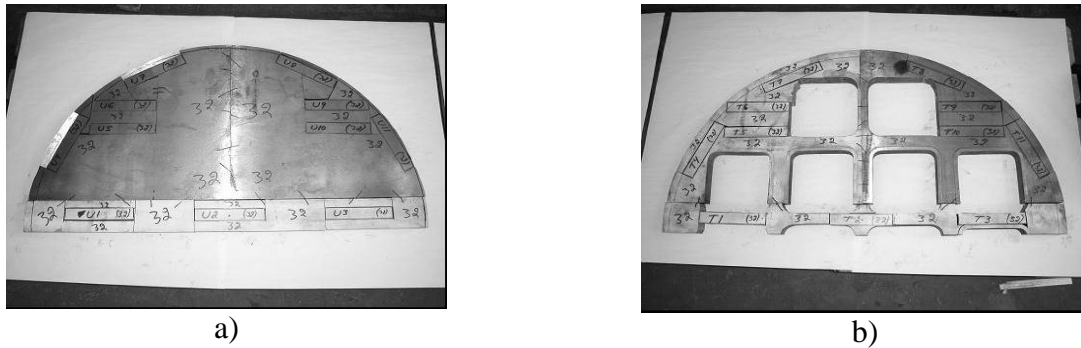

a)   b)

Figure 1. Cut segment for specimen preparation a) bottom (solid) and b) top (with channels)

Tensile and Fracture Tests

There was generally very good agreement between test data derived by the different organizations [3],[4]. Figure 2 shows mean value and standard deviations for elongation at fracture for specimens from the three inserts taken from the bottom and two orientations in the upper part of the insert. It is apparent that there is a large variation in ductility between the three inserts as well as within inserts and that the original 11% strain criterion is generally not satisfied. Insert I25 had the smallest variation in elongation at fracture. For inserts I25 and in particular I24 specimens taken from the bottom of the insert had higher elongation than specimens taken from the top.
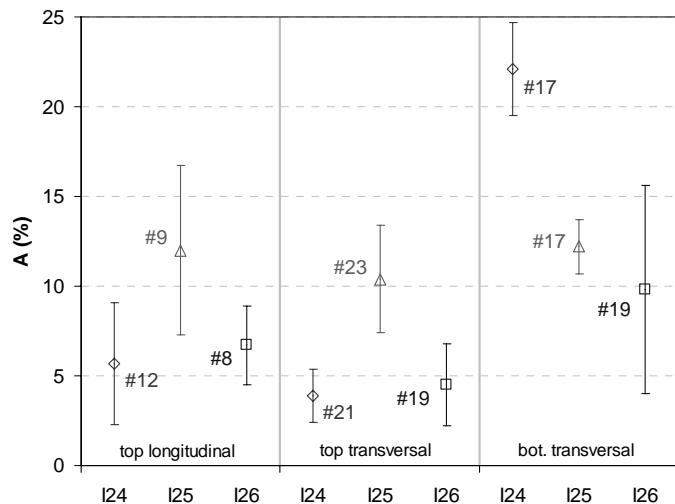

Figure 2. Elongation after fracture: mean values and ± standard deviation plotted for i) canister insert (I24, I25, I26), ii) sampling region (top, bottom) and iii/ specimen orientation. # indicates the number of tests per set.

The stress-strain curves for different specimens from the same insert were almost identical until fracture. Insert I26 had more hardening than I24 and I25 (who had almost identical stress–strain curves). The fracture tests indicated some variation in the fracture toughness for crack growth initiation, J_{IC}, between inserts. Mean values were 47, 58 and 32 kN/m with standard deviations 10, 9 and 5 kN/m for I24, I25 and I26 respectively. All inserts had significant crack growth resistance. The crack growth resistance curves were fitted to the formula

$$J_R(da) = J_{IC} + e^{a_3 + a_2 \ln(da) + a_1 (\ln(da))^2} \tag{1}$$

2

the values for a_1, a_2 and a_3 were (-0.069, 0.462, 3.66), (-0.094, 0.420, 3. 84) and (-0.090, 0.494, 3.13) for the inserts I24, I25 and I26 respectively.

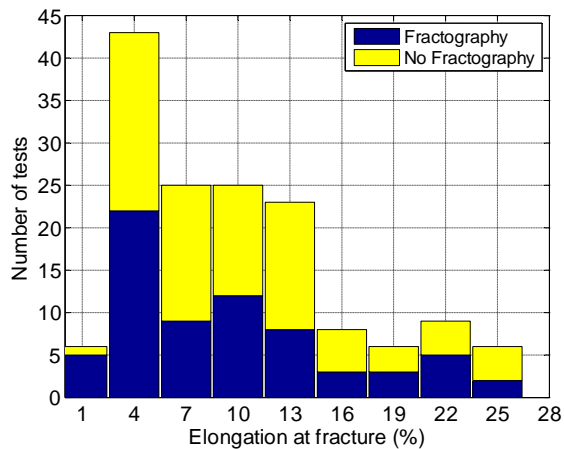Fractographic and Metallographic Analysis of Tensile Specimens

Figure 3. Histogram of tested specimen and the fraction analysed by microstructural analysis
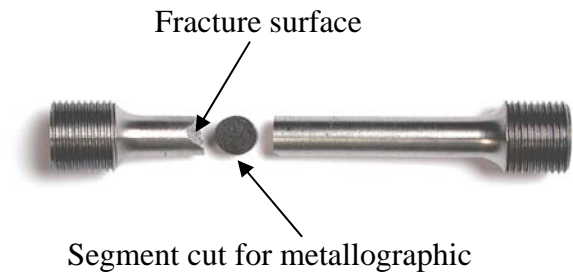

Figure 4. Tensile specimen after test showing fracture surface and segment for microstructural analysis

The assumption is that the large variation in ductility was caused by variation in the material microstructure and by casting defects. Seventy of the tested 150 tensile specimens, Figure 3, were therefore analysed by fractographic analysis of the specimen's fracture surface and by metallographic analysis of a small segment close to the fracture surface shown in Figure 4.

The metallographic analysis was done by high resolution scanning electron microscope (SEM) in back-scattered electrons (BEI) imaging mode [7]. The image analysis of graphite parameters was done by user-developed programmes using routines from MATLAB image processing Toolbox. For each specimen typically 20 images, each with approximately 100 graphite nodules, were used. The individual graphite nodules were characterized in accordance with ISO 945 [8] as graphite type (GT) I, III, IV/V and VI. Figure 5 shows one image with GT-III and GT-VI nodules indicated. This automatic procedure allowed very accurate and objective sizing and categorization.
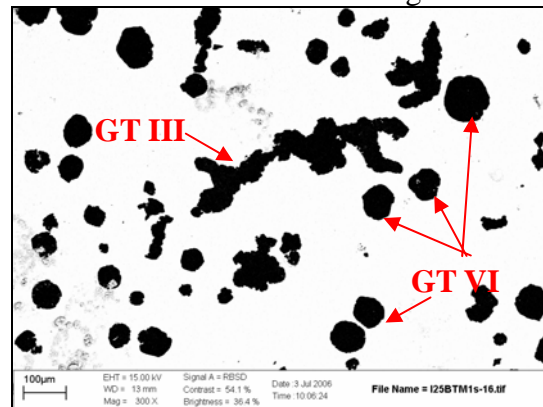

Figure 5 Graphite nodules from specimen with GT III and VI indicated.

The fractographic analysis of fracture surfaces was done by the same SEM but using secondary electrons imaging (SEI) mode to reveal surface morphology and casting defects and BEI mode to identify matrix, graphite, secondary phase, inclusions and impurities. X-ray dispersive analysis (EDS) was used to determine the chemical composition of the casting defects. The microstructural analyses in the previous investigations [3], [4] were done by semi manual methods, which is less reliable. The fracture surfaces contained different types of casting defects of varying sizes. The most typical casting defects was in-situ oxide films of type $(Mg\text{-}Si\text{-}Fe)_xO_y$. Figure 6a shows a SEI-macrograph of one fracture surface with a larger and a number of smaller oxide films and Figure 6b shows the image processed picture for defect sizing. The mean aspect ratio a/b of the largest defects was close to 2.
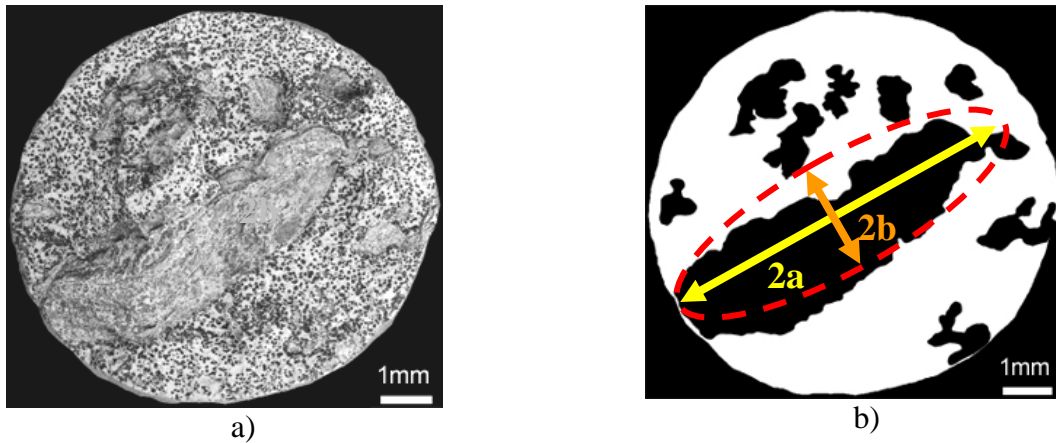
3

a)

b)

Figure 6 Fracture surfaces with casting defects for insert with diameter 9 mm and A = 1.4 % a) SEI macrograph b) processed picture for defect sizing.

Figures 7a and 7b show the measured elongation at fracture versus the maximum feret (2a in Figure 6)). In addition to the maximum feret, the ductility is also affected by the amount of additional casting defects and the shape of the largest defect. In Figure 7a the three symbols represent the largest defect's fraction of the total casting defect area on the fracture surface, whereas in 7b the symbols represent defects with aspect ratio larger and smaller than 2. It follows directly from Figure 7 that the ductility decreases with the casting defect maximum feret. As expected the ductility is generally somewhat lower for specimens for which there is significant amount of other casting defects and higher with increasing aspect ratio.
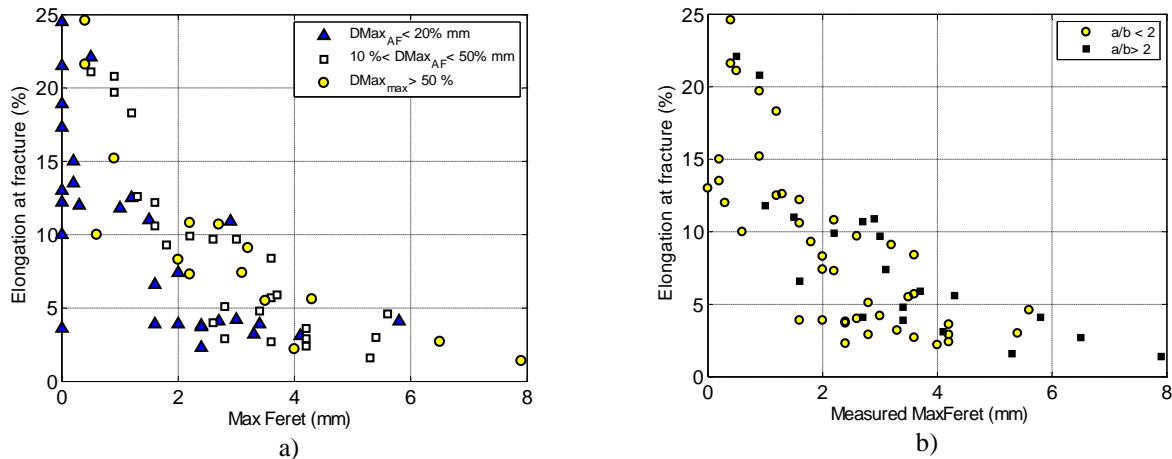

a)

b)

Figure 7 Measured elongation at fracture vs. measured max feret of casting defects a) different values of the largest defects area normalized with total defect area on fracture surface b) different defect aspect ratios

Figure 8a and 8b depict elongation at fracture versus "Bad graphite" on fracture surface and nodularity from the metallographic analysis of the cut-out segment. Nodularity is defined as the area of GTVI normalized with the total area of graphite in the cut out segment. Bad graphite is defined as the total area of III, IV/V and ferrite normalized with the fracture surface area. For each specimen the different symbols are used for large, medium and small largest casting defect on the fracture surface. The first observation is that the casting defects affect the ductility more than nodularity and Bad graphite, but from the small defect data points we can also assess the influence of each of the four graphite properties.
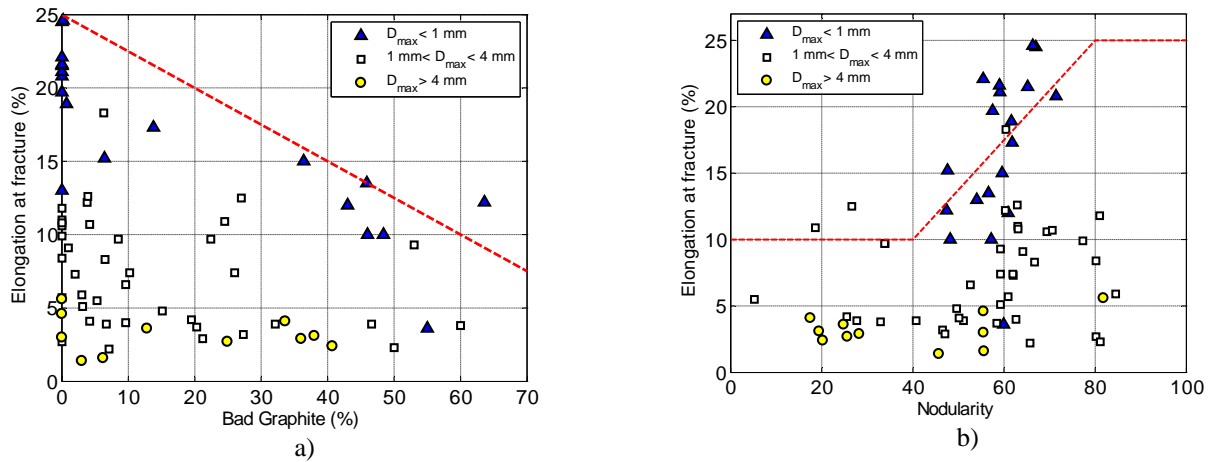
4

Figure 8 Measured elongation at fracture vs. a) Fraction of bad graphite on fracture surface b) nodularity

MODELLING OF TENSILE TESTS

Empirical relationships can be estimated between graphite properties and elongation at fracture using the "small defect" data points in Figure 8. The red lines in Figure 8a and 8b are linear and bi-linear trend curves:

$$A_{Nod} = 10 \; Nodularity < 40, 10 + (Nodularity - 40) \cdot 25/40, 25 \; Nodularity > 80 \Big\}$$

$$A_{BG} = 25 - Bad \; Graphite/4 \qquad\qquad\qquad\qquad\qquad\qquad\qquad (2)$$

Deterministic Fracture Analysis for Oxide Film Defects

The oxide films are initially closed but open up and act as cracks when the material is loaded in tension. Our assumption is that fracture is caused by the largest defect in the specimen. An elastic plastic FE-model of a tensile specimen with a penny shaped crack of radius a, with the crack surfaces normal to the loading was used to model the tensile tests. The stress-strain curves were taken directly from the tensile tests and fitted to Ramberg-Osgood deformation plasticity model. The J-integral was computed as function of the applied load for different crack sizes. The J-value was almost linear vs. applied engineering strain, ε_0 and slightly non-linear with defect size, a, and therefore fitted to the simple linear equation,

$$J(\varepsilon_0; a) = c \cdot \varepsilon_0 \cdot a . \qquad\qquad (3)$$

The coefficient c depends on the stress-strain curve and is determined by making a least-square fit with the computed J-values. The applied strain for initiation of crack growth for a specific crack size and fracture toughness value, J_{IC}, can be determined from Eq. (2) as,

$$\varepsilon_{cr}^i(J_{IC}; a) = J_{IC}/(c \cdot a) \qquad\qquad (4)$$

For very short cracks, the critical strain as well as the derivative, $dJ/da = c\varepsilon_0$, are quite high and unstable crack growth is expected, whereas for larger cracks they are low and some stable crack growth is expected as long as
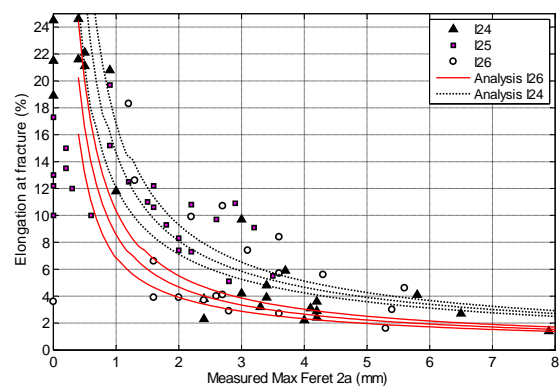

Figure 9 Measured and computed elongation at fracture vs. Max Feret of largest casting defect

5

$dJ/da < dJ_R/da$. The strain at which instability would occur, ε_{cr}^R, and the associated amount of stable tearing, Δa, can be computed from Eq. (3) and (4) and the crack growth resistance curve, Eq. (1),

$$\left.\begin{aligned}\varepsilon_{cr}^R(a) &= \frac{dJ_R(\Delta a)}{da}/c \\ \Delta a &= \frac{J_R(\Delta a)}{c\varepsilon_{cr}^R} - a_0\end{aligned}\right\}. \qquad (5)$$

As mentioned above the casting defects had typically an aspect ratio of 2. For the elastic case, the ratio for maximum value of J for an elliptic defect with aspect ratio a/b, ($b < a$) and a circular is with radius a is given by [9],

$$\frac{b}{a}/\left(\int_0^{\pi/2}\sqrt{1-\left(1-b^2/a^2\right)\sin^2\varphi}\,d\varphi\right)^2 \qquad (6)$$

Figure 10 Computed crack growth resistance at unstable crack growth versus original defect size

For $a/b = 2$ this factor is 0.84. This correction factor has been applied to Eq. (3) in the analysis below unless otherwise stated. Computed curves for I26 and I25 are shown in Figure 9 along with the measured data. The fracture toughness values correspond to the mean value and ± one standard deviation for insert I26 and I24 respectively. Figure 10 shows the computed fracture toughness at crack instability versus the initial defect size for the three inserts.
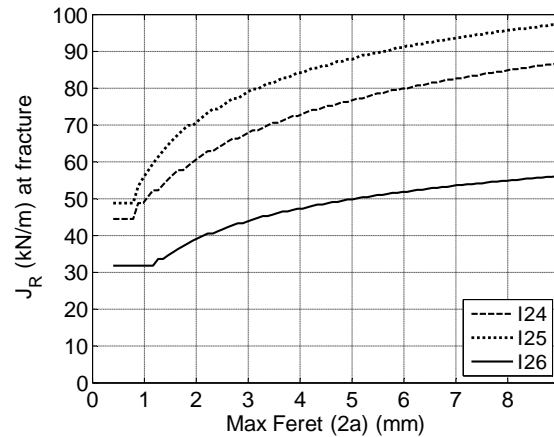
If the different casting defects have been quantified and sized and the microstructure is known, then the elongation at fracture can be inferred from the failure mode with the lowest failure strain. Figure 11 depicts the computed versus the measured elongation at fracture for the four different failure modes using this "weakest link" approach and with the aspect ratio factor for each crack. The overall agreement is rather good but there is quite a bit of scatter.
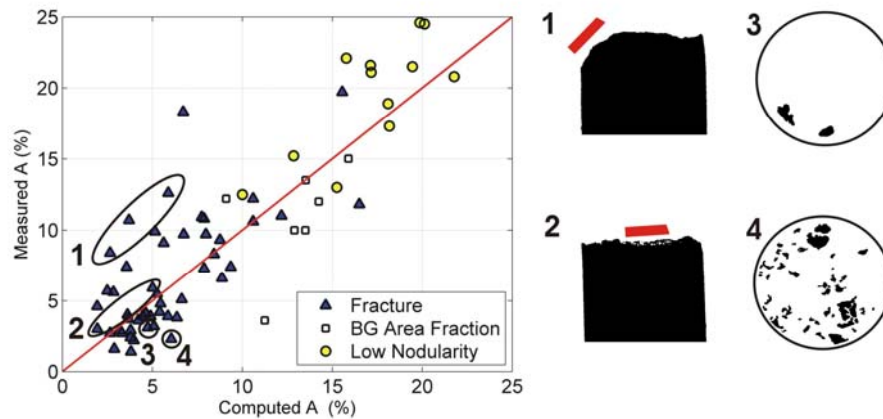
Figure 11 Computed vs. measured elongation at fracture for different failure modes. The Figures 1 and 2 show defect orientation and 3 and 4 overall defect distribution on fracture surface.

In the analysis we assume that defects are oriented such that the crack surface is normal to the applied loading. To investigate if this could explain some of the conservative predictions the orientation of the initial defect was checked for three specimens for which predicted elongation was lower than the measured (1) and three for which the agreement was very good (2). The angle

for the three specimens in "Set 1" was between 30° and 45°, whereas for the three specimens in "Set 2" the angle was between 0° and 20°. The presence of multiple defects, as indicated in Figure 7b, could be one source for underprediction of the ductility. This was also supported by looking at fracture of two specimens shown in Figure 11 (Set 3 and 4).

Probabilistic Fracture Analysis

The cracked body FE-results were used in a probabilistic fracture mechanics framework assuming an exponential size distribution of equally shaped cracks,

$$f_a(a) = e^{-a/\bar{a}}/\bar{a} \quad \text{and its integral} \quad F_a(a) = 1 - e^{-a/\bar{a}} \tag{7}$$

Such distribution has been supported by inspection of nuclear steels [10] and has also been verified for ductile cast iron in a large Scandinavian study [11]. The mean defect size, $\bar{a}$, and the number of defects in a given reference volume, N_v, will be determined from tensile test data. The failure probability may be computed from the integral,

$$p_f = \int_0^\infty F_{J_{IC}}(x) f_J(x) dx, \tag{8}$$

where $F_{J_{IC}}$ is the cumulative distribution function for the fracture toughness and f_J the density function for J. For a single crack this is given by:

$$f_J(J) = f_a(a) \cdot |da/dJ| = \frac{e^{\frac{-J}{c\bar{a}\varepsilon_0}}}{c\varepsilon_0\bar{a}}. \tag{9}$$

The variation in fracture toughness has a much smaller impact than the variation in defect size for the ductility [3]. As a first approximation we assume the fracture toughness to be invariant for a specific insert. The probability function, Eq (8), can then be integrated directly,

$$p_f(J; \varepsilon_0) = \int_{J_C}^\infty f_J(x) dx = e^{\frac{-J_C}{c\varepsilon_0\bar{a}}} \tag{10}$$

The probability density function for the strain variation, f_ε, is determined by differentiation of Eq. (10) with respect to ε_0.

$$f_\varepsilon(\varepsilon_0; J_C) = \frac{J_C}{c\bar{a}\varepsilon_0^2} e^{\frac{-J_C}{c\bar{a}\varepsilon_0}} \tag{11}$$

In the fracture model specimens only fail when defects become critical. Thus when defects become vanishingly small the elongation at fracture becomes unbounded. In the tests specimens also failed by other mechanisms and the elongation never exceeded 25%. We therefore define an upper bound for the strain, ε_{Tr}. The probability function, Eq. (10), must equal unity when integrated from 0 to ε_{Tr}. This is achieved by imposing a truncation factor equal to $Tr = \exp(J_c/(c\bar{a}\varepsilon_{Tr})$ on f_ε in Eq. (11). The probability functions above assume one defect in the reference volume. We assume that there may be N_v defects, each with failure probability p_f^1. The probability that none of the defects becomes critical is then $(1 - p_f^1)^{N_v}$. The probability for at least one defect being critical is then given by,

$$p_f^N = 1 - (1 - p_f^1)^{N_v}. \tag{12}$$

The mean defect size, $\bar{a}$ is determined by calibrating the computed distribution with the measured median failure ($p_f^N = 0.5$) and the number of defects by calibrating with the measured 10 percentile ($p_f^N = 0.1$).

The probability density function, f_ε, and its integral were computed by MATLAB routines for each of the inserts following the procedure outlined above. The measured and computed probability density function for insert I26 and I24 are shown in Figure 12. The model gives an excellent fit. For I24 the top and bottom slab need to be treated separately since the behaviour is quite different and ductility is controlled by defects only in the top part.
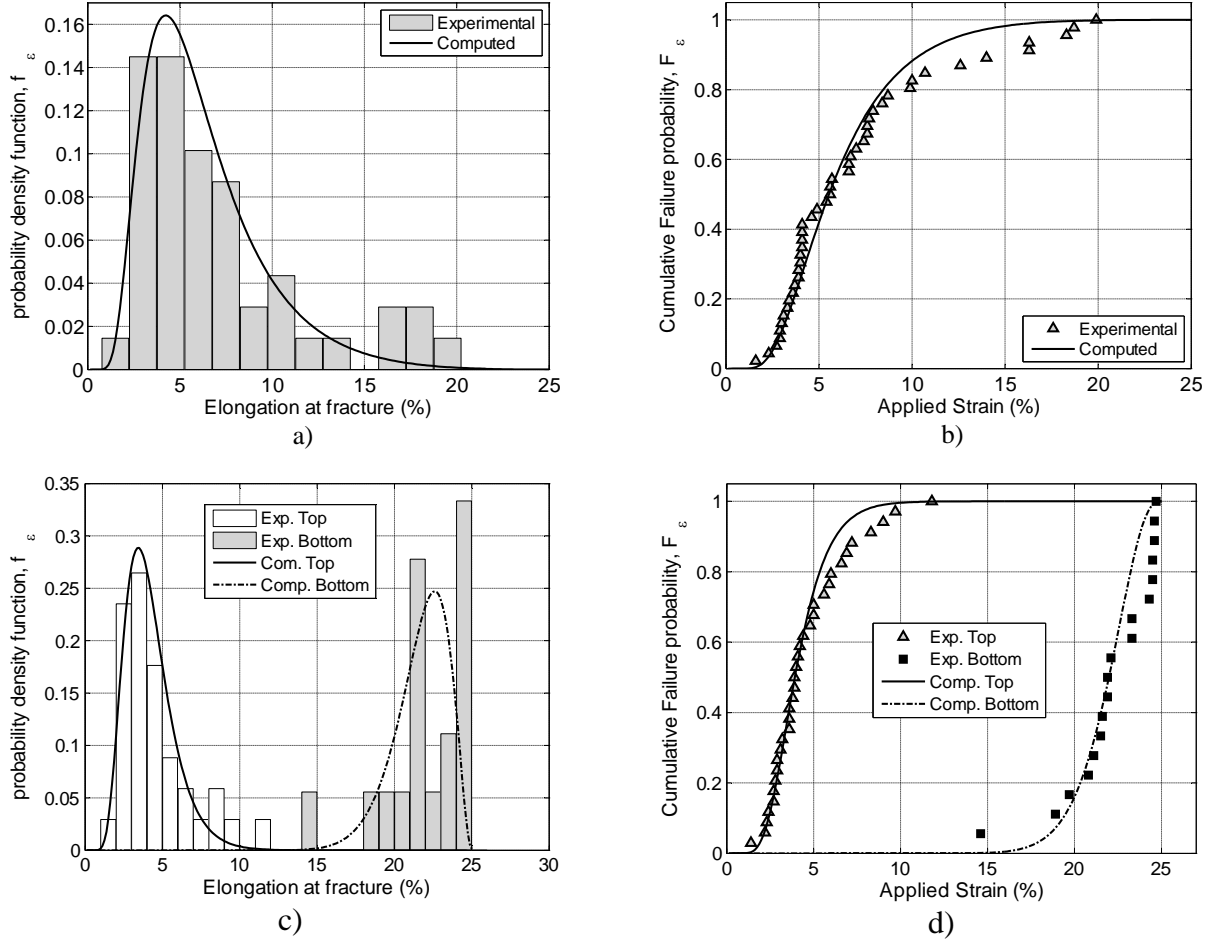

Figure 12 I26 Measured and computed distribution for elongation at fracture a) pdf I26 b) cdf I26 c) pdf I24 Top and Bottom d) cdf I24 Top and Bottom

It follows from the equations above that the distribution functions are independent of the fracture toughness; but that the mean defect size depends linearly on the adopted Jc. The probability that a defect in a specimen is larger than a specific size, a^*, is given by $1 - F_a(a^*)$, which equals $e^{-a^*/\bar{a}}$. The probability that there is at least one defect larger than a^* in a volume with N_v defects is $p = 1 - (1 - e^{-a^*/\bar{a}})^{N_v}$. The probability of having at least N^* specimen out of N_s specimens with maximum feret larger than a^* is given by the cumulative binomial distribution,

$$P(n > N^*) = 1 - \sum_{k=N^*+1}^{N_s} \binom{N_s}{N^*} p^k (1-p)^{N_s - k} \quad where \quad p = 1 - (1 - e^{-a^*/\bar{a}})^N \tag{13}$$
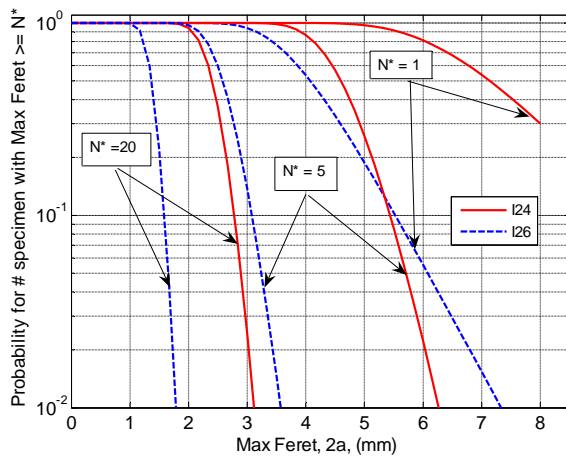
Figure 13 Computed probability for having at least N* = 1, 5 and 20 defects versus defect size I24 Top and I26
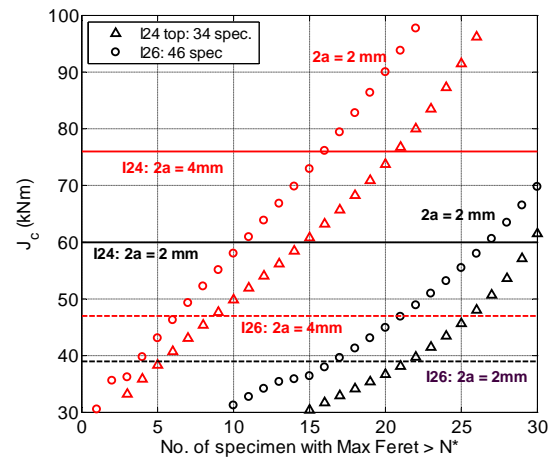
Figure 14 Computed 50% probability for number of specimens with Max feret larger than 2 mm and 4 mm respectively versus fracture toughness for insert I26 (46 spec) and I24 top slab (34 spec)

Figure 13 shows the computed probability for having 1, 5 and 20 specimens versus defect size for I26 with 46 specimens and for the upper part of insert I24 with 34 specimens. The results are based on the fracture toughness for initiation, J_{IC}. From Figure 9 we see that there were 8 specimens with maximum feret larger than 4 mm for I24 top slab and 4 specimens from I26. Since we have analysed only half the specimen we would expect that the total number of defects for the complete set would be about twice this value. The probability curves in Figure 13 suggest a much lower probability. For instance the probability for having 5 defects larger than 4 mm is less than 1% for I26. As mentioned above, the estimated defect size is affected by the fracture toughness. We know from Figure 10 that there is significant crack growth resistance. Figure 14 shows the computed 50% probability for number of specimens versus the fracture toughness value. Results are shown for defect size 2mm and 4 mm for I26 and I24 Top. For a defect with size 2mm the J_R value is 60 and 39 kN/m for I24 and I26 respectively and for 4mm defects it is 76 and 47 kN/m. These are indicated in Figure 14 as well. The predicted number of defects for I24 top larger than 2 and 4 mm are 30 and 21. This should be compared with estimated experimental value of 28 and 16. For I26 the predicted number of defects larger than 2 mm and 4 mm are 15 and 6. For estimated experimental values are 24 and 8.

CONCLUSIONS

This paper has presented an experimental and numerical analysis to relate the variation in ductility in ductile cast iron to casting defects and material microstructure. The following conclusions can be drawn:

- − Casting defects in the form of magnesium oxide film is the dominant contributor to reduction in ductility for the investigated inserts.
- − Specimens/components for which the defects and microstructure have been sized show that the ductility variation can be predicted by fracture mechanics.
- − Statistical distributions of defects can be computed from distribution of elongation at fracture from tensile tests using probabilistic fracture mechanics methodology.

ACKNOWLEDGMENTS

REFERENCES

[1] Andersson C-G. et al., (2005), *Probabilistic analysis and material characterisation of canister inserts for spent nuclear fuel - summary report*, SKB Technical Report TR-05-17., Swedish Nuclear Fuel and Waste Management Co

[2] Nilsson K-F et al., *A probabilistic methodology to determine failure probabilities and acceptance criteria for the KBS-3 inserts under ice-age load conditions*. To appear in Nuclear Technology.

[3] Nilsson K-F, Blagoeva D and Moretto P, "An experimental and numerical analysis to correlate variation in ductility to defects and microstructure in cast iron components", *Engineering Fracture Mechanics*, 2006, **73**, 1133-1157.

[4] Minnebo P., Nilsson K.-F. and D. Blagoeva, (2005), *Tensile, compression and fracture properties of thick-walled ductile cast-iron components*. J. Materials Engineering and Performance, 2006, **16**, 35-45

[5] Annual Book of ASTM Standards 2002 (Section 3, Volume 03.01)

[6] *Tensile Testing of Metallic Material_part 1: Method of Test and Ambient Temperature, EN10002-1:1990,* European Committee for Standardization.

[7] Vokál V., Nilsson K-F and Minnebo, P., 2007, "Characterization of defects and graphite types in ductile cast iron by image processing and its relation to mechanical properties", to appear in *Kovove Mater.*

[8] ISO 945: Designation of Microstructure of Cast Irons – Part 1: Graphite Classification by Visual Analysis (ISO/DIS 945-1:2006), European Committee for Standardization

[9] Tada H., (1985) The Stress Analysis of Cracks Handbook, 2nd Ed. St. Louis, Missouri, USA, Paris productions Inc

[10] Simonen FA, Schuster GJ, Doctor SR and Dickson TL, 2002, Distributions of Fabrication Flaws in Reactor Pressure Vessels for Structural Integrity, Fatigue Fracture and Damage Analysis, ASME PVP-Vol 443-2, pp. 133-143

[11] Hamberg K, Chalmers University of Technology, Dep. of Materials and manufacturing Technology, Göteborg, Sweden private communication.